How to cite: *Angew. Chem. Int. Ed.* **2023**, *62*, e202309318
doi.org/10.1002/anie.202309318

Systems Chemistry

The Role of Chemically Innocent Polyanions in Active, Chemically Fueled Complex Coacervate Droplets

*Fabian Späth, Anton S. Maier, Michele Stasi, Alexander M. Bergmann, Kerstin Halama, Monika Wenisch, Bernhard Rieger, and Job Boekhoven**

Abstract: Complex coacervation describes the liquid-liquid phase separation of oppositely charged polymers. Active coacervates are droplets in which one of the electrolyte's affinity is regulated by chemical reactions. These droplets are particularly interesting because they are tightly regulated by reaction kinetics. For example, they serve as a model for membraneless organelles that are also often regulated by biochemical transformations such as post-translational modifications. They are also a great protocell model or could be used to synthesize life–they spontaneously emerge in response to reagents, compete, and decay when all nutrients have been consumed. However, the role of the unreactive building blocks, e.g., the polymeric compounds, is poorly understood. Here, we show the important role of the chemically innocent, unreactive polyanion of our chemically fueled coacervation droplets. We show that the polyanion drastically influences the resulting droplets' life cycle without influencing the chemical reaction cycle–either they are very dynamic or have a delayed dissolution. Additionally, we derive a mechanistic understanding of our observations and show how additives and rational polymer design help to create the desired coacervate emulsion life cycles.

Introduction

Liquid-liquid phase separation of oppositely charged species is a process that is omnipresent in biological systems yielding droplets that are present in cells[1] referred to as biomolecular condensates. Their properties and aging phenomena are often regulated by biochemical non-equilibrium reactions,[2] resulting in behavior unparalleled by their in-equilibrium counterparts.[3] Yet, the underlying mechanisms remain poorly understood.[4] Besides, theoretical work showed that droplets formed by materials subject to non-equilibrium chemical reaction cycles—and thereby a constant turnover—can show life-like behavior like self-division, regulated growth, or suppressed Ostwald ripening.[5] Such coacervate droplets have also been recognized as potential protocells that functioned as the first containers to concentrate reagents at the early stages of the emergence of life.[6]

Thus, synthetic models for droplets regulated by chemical reaction cycles can unveil new behavior and elucidate their dynamic properties.[7] Such chemically regulated phase-separated droplets can also help us understand their role as protocells at the origin of life or be a step toward synthetic life. In addition to a growing number of examples of carbodiimide fueled assemblies[8] and motors,[9] we recently introduced a chemically fueled reaction cycle that regulates molecular assembly,[10] DNA-duplex formation,[11] and complex coacervation of a cationic peptide with polyanions.[12] The cycle activates a peptide by converting two negatively charged carboxylates into their corresponding anhydride by a carbodiimide activation reaction (Scheme 1).[12a,b] In this context, we refer to the carbodiimide as a fuel as it is converted in the activation reaction. The activated peptide is short-lived as the anhydride spontaneously deactivates through hydrolysis, yielding the original peptide. The zwitterionic peptide has an overall charge of $+1$. It only weakly interacts with polyanions, whereas the short-lived activated peptide is cationic with an overall charge of $+3$ and can thus bind polyanions to form droplets. Our platform serves as a model system for synthetic protocells that emerge, divide, and decay at the expense of simple chemical fuel.[12a] Besides, new non-equilibrium dynamic behavior in these chemically fueled emulsions, including the formation of spherical shells as a non-equilibrium steady state morphology, can be observed.[12e]

In these chemically fueled coacervates, the polyanion is a passive component. However, its influence on the droplet's behavior is seemingly overlooked and scarcely investigated. Understanding polyanion's role enables the creation of systems that are fully dynamic, metastable, or even in an arrested state without the need to change the kinetics of the reaction network. Such studies would aid protocell studies, for example, by understanding how the lifetime of a droplet varies with the polyanion nature. Besides, such studies help

[*] F. Späth, M. Stasi, A. M. Bergmann, M. Wenisch, J. Boekhoven
Department of Chemistry
School of Natural Sciences, Technical University of Munich
Lichtenbergstrasse 4, 85748 Garching (Germany)
E-mail: job.boekhoven@tum.de
A. S. Maier, K. Halama, B. Rieger
WACKER-Chair of Macromolecular Chemistry
Catalysis Research Center, Technical University of Munich
Lichtenbergstrasse 4, 85748 Garching (Germany)

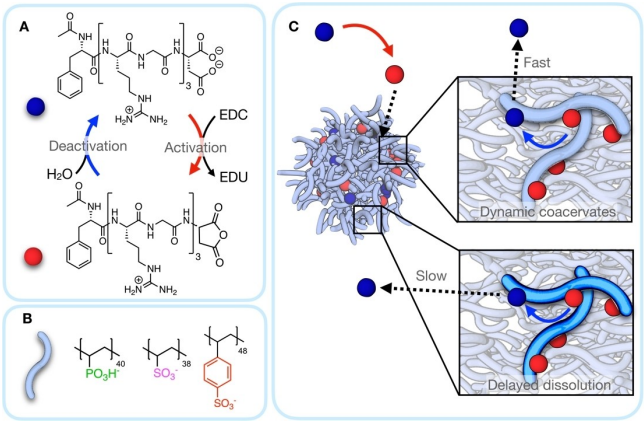

Scheme 1. Polyanions and peptides for chemically fueled complex coacervation. A. The reaction of the carbodiimide EDC with an aspartic acid residue on the C-terminus of a peptide with cationic arginine units reversibly screens two negative charges. This activated peptide—the aspartic anhydride peptide—can complex with polyanions (B) to form complex coacervate droplets (C). The constant turnover of the hydrolytically unstable anhydride in aqueous buffer results in a limited lifetime of the droplets. In this work, the polyanions PSS (red), PVS (magenta), and PVPA (green) are combined with the peptide AcF-$(RG)_3$D–OH and the fuel and the properties of the resulting coacervates are compared. The polyanion choice directly affects the droplet dissolution whenever the precursor-polyanion interactions are too strong.

develop dynamic droplets whose properties like size and ripening dynamics are controlled by reaction kinetics.

In this work, we systematically investigate the role of the polyanionic components in our chemically fueled coacervate droplets and elucidate how they affect the droplet's life cycle. We applied three different polyanions and investigated the role of the peptide-polymer interaction in detail, showing how to tune it systematically to control the outcome of the coacervation reaction cycle.

Results and Discussion

The chemically fueled complex coacervate-based droplets we study here are based on a previously published peptide design AcF$(RG)_3$D–OH in which three arginine-glycine repeat units provide three cationic residues. The C-terminal aspartic acid partly negates these charges resulting in a zwitterionic peptide with an overall charge of +1 (Scheme 1A). The peptide can be chemically activated for coacervation by reacting with the carbodiimide EDC (1-ethyl-3-(3-dimethylaminopropyl) carbodiimide, fuel). Upon activation, the fuel converts the C-terminal aspartic acid into its corresponding anhydride. The activation negates the two anionic carboxylates and thereby increases its overall charge to +3, which increases its interaction strength with polyanions.[12b] A deactivation reaction reverts the activated peptide to the original peptide through anhydride hydrolysis. The half-life of the activated peptide is about 82 seconds. Thus, upon application of fuel to the peptide, a reaction cycle commences that transiently activates peptides and increases their ability to bind polyanions.

We combine this peptide design with three types of polyanions of comparable size, i.e., poly(styrene sulfonate) (PSS_{48}), poly(vinyl sulfonate) (PVS_{38}), and poly(vinyl phosphonic acid) ($PVPA_{40}$) (Scheme 1B). PSS and PVS are commercially available, whereas PVPA was synthesized by REM-GTP (Rare Earth Metal-Mediated Group-Transfer Polymerization) of diethyl vinyl phosphonate followed by deprotection of the phosphonate diester (see Supporting Information for details).[13] All of these polyanions, also PVPA, comprise monoacidic units under our working condition of pH 5.3.[14] The minor differences in their chain length are not expected to influence the coacervate droplet properties.[12b]

We combined the peptide with each polyanion, and we monitored the evolution of turbidity in response to the chemical fuel. In this context, turbidity is a measure of the presence of the droplets. The overall lifetime of the population of droplets produced can also be determined with such experiments. We used 23 mM peptide, 15 mM EDC, and 4.1 mM polyanion expressed as the concentration of monomers in 200 mM MES buffered at pH 5.3. Despite the very similar compositions of the experiments, we found the turbidity evolved differently. The lifetimes of the population of droplets were 8 minutes for PVPA, 13 minutes for PVS, and 17 minutes in the case of PSS (Figure 1A). These observations suggest that the polyanion, which should not affect the reaction cycle, plays an important role in the behavior of the droplets.

We determined whether the polyanion influenced the chemical reaction cycle that governs these properties. We

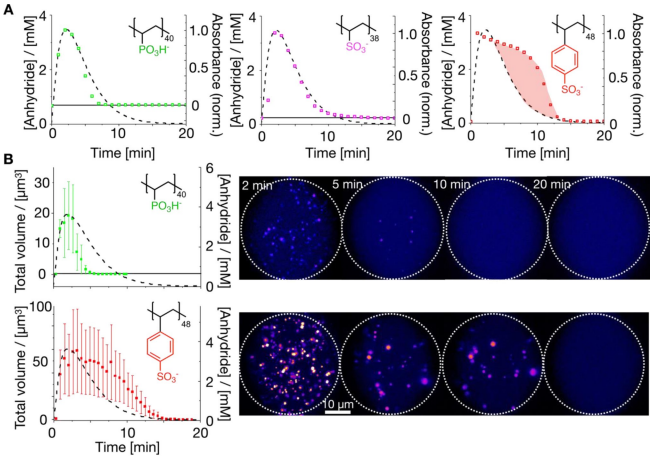

Figure 1. The different polymers affect the droplet lifetimes. A. Overlays of the turbidity traces above the CCC thresholds of different polyanions ($PVPA_{40}$ green, PVS_{38} magenta, PSS_{48} red) with the respective anhydride evolution over time (23 mM AcF$(RG)_3$D–OH, 15 mM EDC, 4.1 mM polyanion expressed in monomer units, 200 mM MES buffer at pH 5.3). B. Microfluidic analysis of the total coacervate volume evolution for $PVPA_{40}$ (green) and PSS_{48} (red) and exemplary images of the droplets over time (PVPA upper row, PSS below). Sulforhodamine B was used as a fluorescent dye at a concentration of 0.2 µM for PSS and 0.6 µM for PVPA samples.

first measured the kinetics of the reaction cycle by HPLC in the presence of the three polyanions. We found that the different polyanions had no significant effect on the kinetics of the reaction cycle (Figure S1). For all polyanions, the EDC was converted in 18 minutes. We used a kinetic model to fit the evolution of the concentration of fuel and activated peptide.[12b] With that kinetic model, we could determine that the activated peptide had a half-life of 82 seconds independent of the polyanion. The finding that the presence of droplets or their composition does not affect the kinetics of the reaction cycle is in line with previously published data.[12a,e] Put differently, the polyanion is seemingly innocent, i.e., it does not affect the chemical reaction cycle which regulates the droplets. Thus, any influence of the polyanion on the behavior of the coacervate droplet can be attributed to its complexation with the peptides.

We first tested if the nature of the polyanion affected the critical coacervation concentration of the activated peptide (CCC). Because the activated peptide is transient, these methods are complicated and subject to hysteresis effects. We, therefore, determined the CCC for the induction of droplets and their dissolution. To do so, we added a batch of fuel and determined by turbidity measurements when droplets were formed and dissolved. We then used the kinetic model to determine the exact concentration of activated peptide at those time points (Figure S2). Droplets were formed when the activated peptide concentration passed 690, 243, or 77 μM for 4.1 mM of PVPA, PVS, and PSS, respectively. Similar values were found for the dissolution threshold concentration for these droplets. These findings suggest that the CCCs differ for various polyanions, but hysteresis, when the system goes through the CCC at dissolution or formation, does not play a large role.

With the kinetic model and the CCC, we could predict the evolution of the reaction cycle and compare it to the evolution of turbidity (Figure 1A). For a fair comparison, we plotted the origin of the turbidity data such that it crosses the CCC of the peptide. When 23 mM peptide was fueled with 15 mM fuel, the turbidity's evolution matched the reaction cycle's evolution almost perfectly for PVPA and PVS. The turbidity and the concentration of activated peptide both peak simultaneously and reach their half-life times, and dissolve when they reach their CCC. In contrast, the evolution of the turbidity of the PSS differs drastically from the reaction cycle. The turbidity peaks slightly early and then decays much slower. Nevertheless, the turbidity is negligible when the concentration peptide falls below the CCC. These observations suggest that PSS droplets dissolve slower than the peptide deactivates, which could be explained by the deactivated peptide not immediately leaving after deactivation. These trends also hold for conditions that yield a significantly higher concentration of activated peptide (16 mM peptide fueled with 50 mM of EDC in the presence of 25 mM polyanion in 200 mM MES at pH 5.3). (Figure S3).

To further understand the relation between droplet behavior and the chemical reaction cycle, we analyzed the individual coacervate's life cycle by confocal microscopy in a microfluidic setup.[12c] In the microfluidic setup, microreactors were prepared by mixing an aqueous stream of polyanion, buffer, and peptide with an aqueous fuel stream. These aqueous flows were mixed and then combined with a perfluorinated oil to yield microreactors with all ingredients for the complex coacervates. The microreactors were trapped in a drop spot chamber, after which imaging was started. Every 17 seconds, the entire microfluidic droplet was imaged by confocal microscopy. With the setup, we could image the nucleation of coacervate-based droplets, their fusion, and, eventually, their dissolution (Figure 1B). We measured the volume of each coacervate-based droplet in each frame in the cycle, from which we calculated the total coacervate volume in the microfluidic droplets. For all polyanions, the total volume rapidly increased after adding the fuel. After a few minutes, it started to decay until all coacervate-based droplets had dissolved. The moment the total volume of droplet material disappeared coincided roughly with when the concentration of activated peptide broke through the CCC.

When we analyzed the evolution of the individual coacervate-based droplets, it became apparent that droplets nucleated within the first minute. From there, their count rapidly decreased because of fusion and dissolution. In the case of PVPA, the dissolution outcompetes fusion after 3 minutes leading to a rapid decrease in the average volume of the droplets. In contrast, the dissolution for PSS is delayed compared to PVPA, and fusion is dominant. Consequently, the average volume of a PSS droplet reaches a maximum later in the cycle and reaches a much higher value. In line with the total volume analysis, the PSS droplets persist longer than PVPA droplets. Thus, from an individual droplet's perspective, the PSS droplets persist longer, have more time to fuse, and reach a much greater final volume (Figure S4).

Our observations have big implications if we consider our compartments the basis for self-sustaining compartments. The appropriate choice of the inert, polymeric droplet scaffold leads to droplets that can better survive starvation periods, i.e., periods without fuel supply. On the other hand, dynamic polymer-peptide combinations like PVPA or PVS are directly susceptible to changes in their building block concentrations. Their properties can be directly correlated to the chemical reaction cycle.

To better understand the mechanism of how the polymers influence the droplet life cycle, we measured the interaction strength of the peptide $AcF(RG)_3D–OH$ and the activated peptide. Because the activated peptide is short-lived, it cannot be used in ITC. Instead, we used a model for the activated peptide $AcF(RG)_3N–NH_2$, i.e., we mutated the anionic aspartic acid for the charge-neutral asparagine. Like the activated peptide, this model peptide also contains two additional cations compared to the precursor while maintaining all other relevant structural features. The model peptide anhydride also shows similar CCC values to the actual anhydride (Figure 2A).

For PVS and PSS, the K_D values of the peptide were more than an order of magnitude higher than that of the model for the activated peptide. Moreover, significantly different K_D values were obtained for the different peptide-

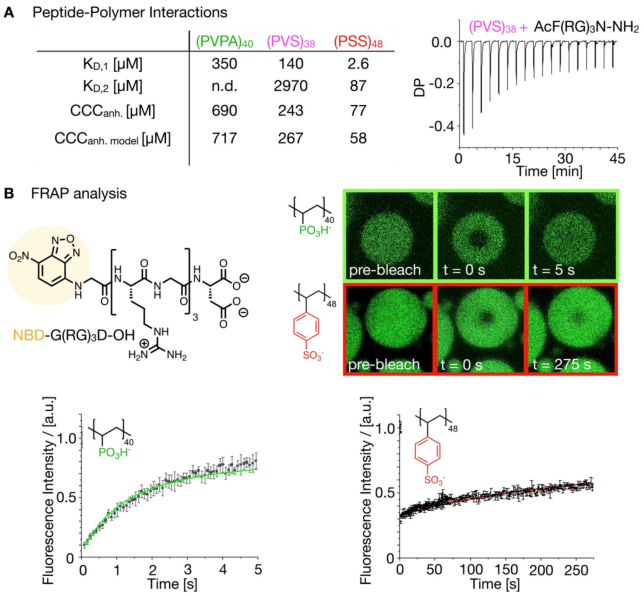

Figure 2. Mechanistic understanding of the polyanion influences. A. K_D values of the different polyanions with the peptide and anhydride model as obtained from ITC analysis. $K_{D,1}$ was obtained with AcF-$(RG)_3$N–NH_2, and $K_{D,2}$ with AcF$(RG)_3$D–OH. Right: Example titration obtained from titrating AcF$(RG)_3$N–NH_2 to PVS_{38}.The CCC values for the peptide anhydride and the anhydride model are in good agreement. B. FRAP experiments with the fluorescently labeled peptide NBD–G-$(RG)_3$D–OH and the polyanions $PVPA_{40}$ (green) and PSS_{48} (red).

polymer pairs, which corroborates the not innocent role of the polyanion (Figure 2A, Figure S5). PSS was interacting by far the strongest with both the model for the activated peptide and the peptide, which we hypothesize is a result of the additional aromatic and cation-π interactions along with a potential contribution of hydrophobic interactions arising from the larger polymer backbone.[15] In contrast, PVPA interacted weakly with the model for the activated peptide and showed no measurable interactions with the peptide. The values for PVS lay between the other two polyanions, which can be attributed to the strong polyelectrolyte character of the sulfonate groups but the missing aromatic interactions that can contribute to the interactions for PSS. For PVS, the interaction with the AcF$(RG)_3$D–OH is already weakened significantly (the K_D value is already 34 times higher than for PSS but still measurable), further hinting at the important role of the precursor for the droplet decay profile. The different K_D values for the polyanion-anhydride model interactions are reflected in the different CCC values for the different polymers.

We used fluorescence recovery after photobleaching (FRAP) experiments to test the precursor's behavior in the droplets. We synthesized a fluorescent analog of the peptide (NBD–G$(RG)_3$D–OH, Figure 2B). The FRAP experiments on in-equilibrium droplets revealed a 1000 times higher diffusion coefficient for the peptide in PVPA ($D = 1\ \mu m^2/s$) than in PSS ($D = 0.001\ \mu m^2/s$). This finding further corroborates the strong interaction of PSS with the precursor molecule, while there is no significant interaction with PVPA.

The high affinity of the peptide to PSS and its low diffusion coefficient in droplets of PSS suggest that the precursor building block is hindered from leaving the droplet phase after the activated peptide deactivates. This mechanism would imply that deactivated peptide accumulates in the droplets, which explains why the decay of the turbidity is delayed compared to the kinetics of the reaction cycle. Indeed, partitioning coefficients of in-equilibrium coacervates prepared from PVPA or PSS in combination with AcF$(RG)_3$D–OH and AcF$(RG)_3$N–NH_2 show a roughly twice as large partitioning of NBD–G$(RG)_3$D–OH in the droplet phase for PSS coacervates than for PVPA (Figure S6A). For the active systems, after fueling with EDC under the same conditions, there was a 5-fold difference in the partitioning coefficients (397.6 ± 131.5 for PSS and 79.0 ± 26.0 for PVPA) at the expected maximum of anhydride concentration (Figure S6B). Taken together, polyanions with a high affinity for the peptide can prevent the peptide from leaving the droplet after deactivation, which leads to delayed dissolution.

Excited by the mechanistic understanding of how polyanions can influence the lifetime of droplets, we sought a method of controlling it. As the underlying mechanism is related to the binding affinity between the peptide and polyanion, the approach is to tune this interaction strength which is possible by adding salt.[16] Indeed, when we add 250 mM of NaCl, we observe a reduced lifetime and a steeper decay profile of the turbidity compared to the system without NaCl. However, there was still a significant amount of hysteresis when comparing the evolution of peptide anhydride and turbidity. After adding 500 mM NaCl, the turbidity closely follows the evolution of the peptide anhydride concentration. These observations suggest that the critical coacervation concentration increases, leading to a shorter lifetime. Besides, the addition of salt leads to a decrease in the interaction strength between the peptide and the polyanion, which yields less hysteresis between the evolution of the anhydride concentration and turbidity. Indeed, an investigation by ITC showed that with as little as 250 mM NaCl, the K_D values for both the peptide and the model of the activated peptide were drastically higher (Figure 3A, Figure S7). Furthermore, the addition of 500 mM NaCl increased the $K_{D,2}$ value further such that it could not be measured anymore. The ITC data suggests that if $K_{D,2}$ is very high or too large to be measured, we can expect droplets whose evolution follows the anhydride profile nicely. Noteworthy, this relation between $K_{D,2}$ and the droplet dynamics also holds for PVS and PVPA without additional salt (Figure 1A).

These observations show that the addition of NaCl can tune the interaction strength. If the interaction strength of the activated peptide and polyanion decreases ($K_{D,1}$), the droplet's lifetime decreases. If the interaction strength of the peptide and the polyanion is decreased ($K_{D,2}$), the evolution of the turbidity follows the evolution of the kinetics of the reaction cycle.

To further corroborate these findings, we measured the diffusivity of the precursor in response to different amounts of salt by FRAP. To perform FRAP experiments, we

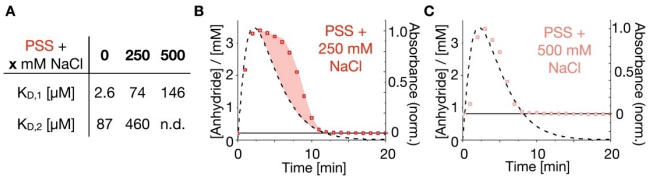

Figure 3. Tuning the droplet dynamics by the addition of salt. A. K_D values of AcF(RG)$_3$N–NH$_2$ ($K_{D,1}$) and AcF(RG)$_3$D–OH ($K_{D,2}$) with PSS with and without NaCl. There was no measurable interaction between the peptide and the polyanion anymore under the applied conditions with 500 mM NaCl. B. Turbidity trace PSS in the presence of 250 mM NaCl (23 mM AcF(RG)$_3$D–OH, 4.1 mM polyanion expressed in monomer units, 200 mM MES buffer at pH 5.3, fueled with 15 mM of EDC) overlayed above the CCC with the respective anhydride evolution from the kinetic model. C. Turbidity trace of PSS coacervates in the presence of 500 mM NaCl under the same conditions, overlayed with the respective anhydride concentration profile above the CCC.

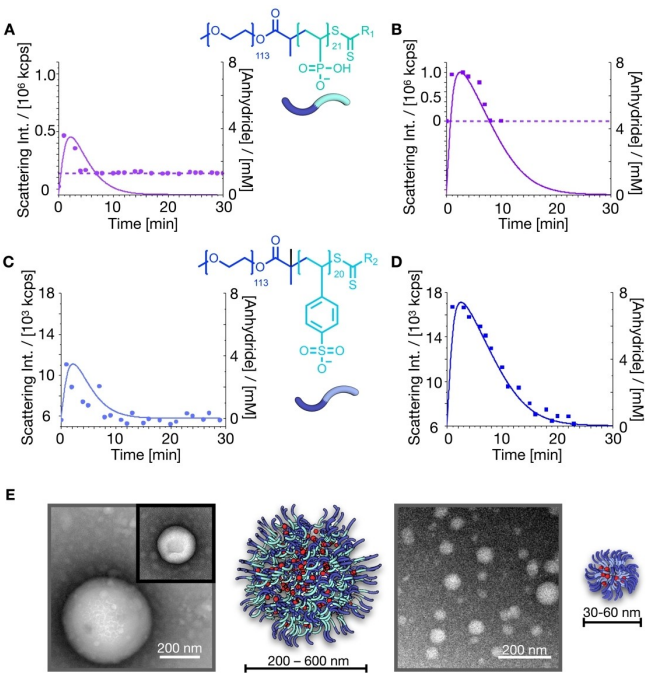

Figure 4. The role of the polyanion in nanosized assemblies/complex coacervate core micelles. A. DLS analysis of PEG-b-PVPA$_{21}$ block copolymers fueled with EDC. 23 mM of AcF(RG)$_3$D–OH were fueled with 15 mM EDC in 200 mM MES buffer at pH 5.3 in the presence of 4.1 mM block copolymer (expressed in monomer units) and the corresponding scattering intensity was followed over time by DLS (left y-axis). The solid lines show the evolution of the anhydride concentration (right y-axis). B. 16 mM AcF(RG)$_3$D–OH was fueled with 50 mM EDC in the presence of 25 mM block copolymer in 200 mM MES pH 5.3. C. and D. Fueling under the same conditions with PEG-b-PSS$_{20}$. **E**. TEM analysis of static samples (8.54 mM AcF(RG)$_3$D–OH, 7.46 mM AcF(RG)$_3$N–NH$_2$, 25 mM block copolymer, all in 200 mM MES at pH 5.3) after staining with uranyl acetate. Left: PEG-b-PVPA$_{21}$. Right: PEG-b-PSS$_{20}$. R$_1$=–O–C$_2$H$_5$ and R$_2$=–S–C$_{12}$H$_{25}$.

created static droplets with our anhydride model in the presence of 500 mM and 1 M NaCl. The experiments revealed diffusion coefficients of $D = 0.003\ \mu m^2/s$ in the presence of 500 mM NaCl and $D = 0.0043\ \mu m^2/s$ in the presence of 1 M NaCl, showing a 3- to 4-fold increase in diffusivity for the AcF(RG)$_3$D–OH peptide (Figure S8B) in comparison to PSS coacervates without any additional salt (Figure 2B right). This suggests that adding sodium chloride to the chemically fueled coacervation system reduces the half-life times by reducing the polyanion-inactivated peptide interactions, leading to a steeper decay profile by increasing the peptide's diffusivity. This destabilizing effect of NaCl on the coacervate droplets is also observed under higher fuel and building block concentrations (Figure S8A). Overall, the addition of salt to our coacervate droplets is indeed a valid tool to increase the dynamics of the system by closing the gap between peptide anhydride dissolution and droplet decay and they underline the importance of the precursor-polymer interactions further.

From the above study, we conclude that a high interaction strength between the peptide precursor and the polyanion decreases the peptide's diffusivity and thereby hinders the deactivated peptide from leaving the droplet, leading to a measurable delay in the coacervate dissolution. Following this logic, the smaller the coacervate droplets, the smaller the delay in the dissolution should be.

To test this hypothesis, we synthesized block copolymers of PEG and the respective homopolymers of PVPA and PSS via RAFT polymerization (see Supporting Information).[17] These block copolymers formed assemblies with our peptide after adding EDC, as evidenced by DLS analysis (Figure 4A–D). TEM analysis revealed that both block copolymers formed spherical structures when combined with our peptide anhydride model (Figure 4E). For PEG-b-PVPA, the spherical assemblies were polydisperse with a diameter of up to 400 nm. PEG-b-PSS, on the other hand, assembled into smaller, spherical assemblies than the PEG-b-PVPA structures. These initial observations point towards the formation of large compound micelles for both block copolymers. The size differences between the assemblies are also corroborated by DLS and confocal microscopic analysis (Table S1 and Figure S9). They could be related to the higher interaction strength between the peptide and the PSS block than the PVPA block. Similar studies suggest that a lower binding strength leads to a looser packing of the core and, thus, larger assemblies.[18]

In the chemically fueled samples, the block copolymer assemblies of PEG-b-PVPA showed similar lifetimes as their dynamic homopolymer coacervates under the same conditions and led to highly turbid samples. Similarly, the PEG-b-PSS assemblies showed no delay in dissolution. This contrasts the dissolution profile of the PSS homopolymer coacervates (Figure S10). ITC analysis for PEG-b-PSS revealed relatively strong binding between the block copolymer and the peptide and peptide anhydride model ($K_{D,1} = 80\ \mu M$, $K_{D,2} = 141\ \mu M$, Figure S11).

Based on these binding constants, we would expect a delayed dissolution for PEG-b-PSS. The fact that we did not observe this delay suggests that both the size of the assemblies and the binding constants must be considered when predicting the polyanion's influence on the assembly's dissolution kinetics. We propose that in the nanometer size regime, the hindered peptide diffusion does not play a role

and does not lead to an overall delayed dissolution even with a high binding constant for the peptide and polyanion (Scheme 2).

Conclusion and Outlook

We studied the role of the polyanion in chemically fueled complex coacervates and conclude that they greatly alter the outcome of the resulting droplets despite not affecting the underlying chemical reaction cycle. We find that polyanions that bind strongly to the precursor tend to form droplets that dissolve with delayed kinetics compared to the reaction cycle. This effect can be negated by tuning the binding constants, for example, by adding salt or changing the design of the polyanion. Moreover, we find that these effects operate on the microscopic scale, meaning that smaller assemblies like coacervate core micelles are not affected.

Our findings have implications for chemically fueled protocell models in which a delay in dissolution can be desired. If a protocell could control the nature of its polyanion, for example, by synthesizing or selecting specific polyanions, it is able to regulate its lifetime and become more resilient to fuel starvation. When dynamic behavior, like size control or self-division, is desired, we offer design considerations for the polyanion too.

Supporting Information

The authors have cited additional references within the Supporting Information.[12b,c,13,17,19]

Acknowledgements

We thank Kathrin Kollmannsberger (TUM) for the assistance with TEM analysis and Marius Braun and Dr. Christopher Synatschke (MPI für Polymerforschung, Mainz) for help with aqueous SEC analysis. The BoekhovenLab is grateful for support from the TUM Innovation Network—RISE funded through the Excellence Strategy. This research was conducted within the Max Planck School Matter to Life, supported by the German Federal Ministry of Education and Research (BMBF) in collaboration with the Max Planck Society. F. S. and J. B. are grateful for funding from the Deutsche Forschungsgemeinschaft via the International Research Training Group ATUMS (IRTG 2022). J. B. is grateful for the funding by the European Research Council (ERC starting grant under 852187), funding by the Deutsche Forschungsgemeinschaft (DFG, German Research Foundation) under Germany's Excellence Strategy (EXC-2094—390783311) and the ORIGINS cluster. A. S. M. is grateful for the generous funding within a Kekulé fellowship from the Fonds der Chemischen Industrie. Open Access funding enabled and organized by Projekt DEAL.

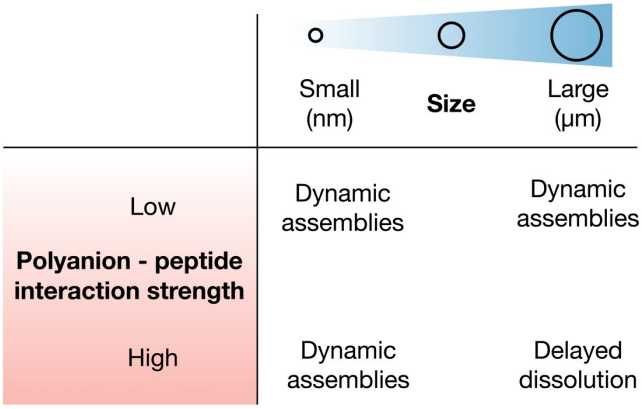

Scheme 2. The different parameters of chemically fueled coacervates that influence their life cycles.

Conflict of Interest

The authors declare no conflict of interest.

Data Availability Statement

The data that support the findings of this study are available from the corresponding author upon reasonable request.

Keywords: Chemically Fueled Coacervation · Membraneless Organelles · Peptides · Polyelectrolytes · Protocells

[1] W. M. Aumiller Jr, F. Pir Cakmak, B. W. Davis, C. D. Keating, *Langmuir* **2016**, *32*, 10042–10053.
[2] a) J. Y. Youn, B. J. A. Dyakov, J. Zhang, J. D. R. Knight, R. M. Vernon, J. D. Forman-Kay, A. C. Gingras, *Mol. Cell* **2019**, *76*, 286–294; b) F. Palangi, S. M. Samuel, I. R. Thompson, C. R. Triggle, M. M. Emara, *PLoS One* **2017**, *12*, e0182059.
[3] a) N. A. Yewdall, A. A. M. André, T. Lu, E. Spruijt, *Curr. Opin. Colloid Interface Sci.* **2021**, *52*, 101416; b) E. Gomes, J. Shorter, *J. Biol. Chem.* **2019**, *294*, 7115–7127; c) R. W. Lewis, B. Klemm, M. Macchione, R. Eelkema, *Chem. Sci.* **2022**, *13*, 4533–4544; d) D. Zwicker, *Curr. Opin. Colloid Interface Sci.* **2022**, *61*, 101606.
[4] W. M. Aumiller Jr, C. D. Keating, *Nat. Chem.* **2016**, *8*, 129–137.
[5] a) D. Zwicker, R. Seyboldt, C. A. Weber, A. A. Hyman, F. Jülicher, *Nat. Phys.* **2017**, *13*, 408–413; b) D. Zwicker, A. A. Hyman, F. Jülicher, *Phys. Rev. E* **2015**, *92*, 012317; c) C. Donau, J. Boekhoven, *Trends Chem.* **2023**, *5*, 45–60.
[6] a) I. Gözen, E. S. Koksal, I. Poldsalu, L. Xue, K. Spustova, E. Pedrueza-Villalmanzo, R. Ryskulov, F. Meng, A. Jesorka, *Small* **2022**, *18*, 2106624; b) S. Koga, D. S. Williams, A. W. Perriman, S. Mann, *Nat. Chem.* **2011**, *3*, 720–724.
[7] N. Martin, *ChemBioChem* **2019**, *20*, 2553–2568.
[8] a) L. S. Kariyawasam, C. S. Hartley, *J. Am. Chem. Soc.* **2017**, *139*, 11949–11955; b) M. M. Hossain, I. M. Jayalath, R. Baral, C. S. Hartley, *ChemSystemsChem* **2022**, *4*, e202200016; c) M. M. Hossain, J. L. Atkinson, C. S. Hartley, *Angew. Chem. Int. Ed.* **2020**, *59*, 13807–13813; d) S. Panja, B. Dietrich, D. J. Adams, *ChemSystemsChem* **2019**, *2*, e1900038; e) J. Sun, J. Vogel, L. Chen, A. L. Schleper, T. Bergner, A. J. C. Kuehne, M. von Delius, *Chem. Eur. J.* **2022**, *28*, e202104116; f) S. Bal, K.

Das, S. Ahmed, D. Das, *Angew. Chem. Int. Ed.* **2019**, *58*, 244–247.

[9] a) S. Borsley, D. A. Leigh, B. M. W. Roberts, *J. Am. Chem. Soc.* **2021**, *143*, 4414–4420; b) S. Borsley, E. Kreidt, D. A. Leigh, B. M. W. Roberts, *Nature* **2022**, *604*, 80–85.

[10] a) M. Tena-Solsona, B. Riess, R. K. Grötsch, F. C. Lohrer, C. Wanzke, B. Kasdorf, A. R. Bausch, P. Müller-Buschbaum, O. Lieleg, J. Boekhoven, *Nat. Commun.* **2017**, *8*, 15895; b) X. Chen, M. Stasi, J. Rodon-Fores, P. F. Grossmann, A. M. Bergmann, K. Dai, M. Tena-Solsona, B. Rieger, J. Boekhoven, *J. Am. Chem. Soc.* **2023**, *145*, 6880–6887; c) J. Rodon-Fores, M. A. Würbser, M. Kretschmer, B. Riess, A. M. Bergmann, O. Lieleg, J. Boekhoven, *Chem. Sci.* **2022**, *13*, 11411–11421; d) F. Schnitter, B. Riess, C. Jandl, J. Boekhoven, *Nat. Commun.* **2022**, *13*, 2816; e) B. A. K. Kriebisch, C. M. E. Kriebisch, A. M. Bergmann, C. Wanzke, M. Tena-Solsona, J. Boekhoven, *ChemSystemsChem* **2023**, *5*, e202200035; f) M. A. Würbser, P. S. Schwarz, J. Heckel, A. M. Bergmann, A. Walther, J. Boekhoven, *ChemSystemsChem* **2021**, *3*, e202100015.

[11] M. Stasi, A. Monferrer, L. Babl, S. Wunnava, C. F. Dirscherl, D. Braun, P. Schwille, H. Dietz, J. Boekhoven, *J. Am. Chem. Soc.* **2022**, *144*, 21939–21947.

[12] a) C. Donau, F. Späth, M. Sosson, B. A. K. Kriebisch, F. Schnitter, M. Tena-Solsona, H. S. Kang, E. Salibi, M. Sattler, H. Mutschler, J. Boekhoven, *Nat. Commun.* **2020**, *11*, 5167; b) F. Späth, C. Donau, A. M. Bergmann, M. Kränzlein, C. V. Synatschke, B. Rieger, J. Boekhoven, *J. Am. Chem. Soc.* **2021**, *143*, 4782–4789; c) A. M. Bergmann, C. Donau, F. Späth, K. Jahnke, K. Göpfrich, J. Boekhoven, *Angew. Chem. Int. Ed.* **2022**, *61*, e202203928; d) C. Donau, F. Späth, M. Stasi, A. M. Bergmann, J. Boekhoven, *Angew. Chem. Int. Ed.* **2022**, *61*, e202211905; e) A. M. Bergmann, J. Bauermann, G. Bartolucci, C. Donau, M. Stasi, A.-L. Holtmannspötter, F. Jülicher, C. A. Weber, J. Boekhoven, *bioRxiv preprint* **2023**, https://doi.org/10.1101/2023.01.31.526480.

[13] a) B. S. Soller, S. Salzinger, C. Jandl, A. Pöthig, B. Rieger, *Organometallics* **2015**, *34*, 2703–2706; b) S. Salzinger, U. B. Seemann, A. Plikhta, B. Rieger, *Macromolecules* **2011**, *44*, 5920–5927.

[14] B. Bingöl, W. H. Meyer, M. Wagner, G. Wegner, *Macromol. Rapid Commun.* **2006**, *27*, 1719–1724.

[15] a) L. Li, A. M. Rumyantsev, S. Srivastava, S. Meng, J. J. de Pablo, M. V. Tirrell, *Macromolecules* **2021**, *54*, 105–114; b) K. Sadman, Q. Wang, Y. Chen, B. Keshavarz, Z. Jiang, K. R. Shull, *Macromolecules* **2017**, *50*, 9417–9426; c) J. Huang, J. E. Laaser, *ACS Macro Lett.* **2021**, *10*, 1029–1034; d) G. Krainer, T. J. Welsh, J. A. Joseph, J. R. Espinosa, S. Wittmann, E. de Csillery, A. Sridhar, Z. Toprakcioglu, G. Gudiskyte, M. A. Czekalska, W. E. Arter, J. Guillen-Boixet, T. M. Franzmann, S. Qamar, P. S. George-Hyslop, A. A. Hyman, R. Collepardo-Guevara, S. Alberti, T. P. J. Knowles, *Nat. Commun.* **2021**, *12*, 1085; e) R. A. Kapelner, V. Yeong, A. C. Obermeyer, *Curr. Opin. Colloid Interface Sci.* **2021**, *52*, 101407; f) U. Lang, E. Müller, N. Naujoks, J. Dual, *Adv. Funct. Mater.* **2009**, *19*, 1215–1220.

[16] a) I. Bos, M. Timmerman, J. Sprakel, *Macromolecules* **2021**, *54*, 398–411; b) D. Priftis, N. Laugel, M. Tirrell, *Langmuir* **2012**, *28*, 15947–15957; c) Q. Wang, J. B. Schlenoff, *Macromolecules* **2014**, *47*, 3108–3116; d) M. Lemmers, J. Sprakel, I. K. Voets, J. van der Gucht, M. A. Cohen Stuart, *Angew. Chem. Int. Ed.* **2010**, *49*, 708–711.

[17] a) K. H. Markiewicz, L. Seiler, I. Misztalewska, K. Winkler, S. Harrisson, A. Z. Wilczewska, M. Destarac, J. D. Marty, *Polym. Chem.* **2016**, *7*, 6391–6399; b) J. M. Ting, H. Wu, A. Herzog-Arbeitman, S. Srivastava, M. V. Tirrell, *ACS Macro Lett.* **2018**, *7*, 726–733.

[18] a) H. M. van der Kooij, E. Spruijt, I. K. Voets, R. Fokkink, M. A. Cohen Stuart, J. van der Gucht, *Langmuir* **2012**, *28*, 14180–14191; b) J. M. Horn, R. A. Kapelner, A. C. Obermeyer, *Polymer* **2019**, *11*, 578.

[19] a) S. Salzinger, B. S. Soller, A. Plikhta, U. B. Seemann, E. Herdtweck, B. Rieger, *J. Am. Chem. Soc.* **2013**, *135*, 13030–13040; b) T. M. Pehl, M. Kränzlein, F. Adams, A. Schaffer, B. Rieger, *Catalysts* **2020**, *10*, 448; c) M. Fuentes-Exposito, S. Norsic, T. Février, P.-Y. Dugas, S. Boutti, S. Devisme, A. Bonnet, F. D'Agosto, M. Lansalot, *Polym. Chem.* **2021**, *12*, 5640–5649; d) D. C. Duffy, J. C. McDonald, O. J. Schueller, G. M. Whitesides, *Anal. Chem.* **1998**, *70*, 4974–4984; e) M. Weiss, J. P. Frohnmayer, L. T. Benk, B. Haller, J. W. Janiesch, T. Heitkamp, M. Borsch, R. B. Lira, R. Dimova, R. Lipowsky, E. Bodenschatz, J. C. Baret, T. Vidakovic-Koch, K. Sundmacher, I. Platzman, J. P. Spatz, *Nat. Mater.* **2018**, *17*, 89–96; f) T. W. Hofmann, S. Hanselmann, J. W. Janiesch, A. Rademacher, C. H. Bohm, *Lab Chip* **2012**, *12*, 916–922; g) A. B. Kayitmazer, H. B. Bohidar, K. W. Mattison, A. Bose, J. Sarkar, A. Hashidzume, P. S. Russo, W. Jaeger, P. L. Dubin, *Soft Matter* **2007**, *3*, 1064–1076; h) F. Schnitter, J. Boekhoven, *ChemSystemsChem* **2020**, *3*, e202000037.

Manuscript received: July 1, 2023
Accepted manuscript online: August 7, 2023
Version of record online: September 6, 2023